Binding of Lead(II), Antimony(III), and Other Isoelectronic Main-Group Ions to Iridium in the Metallomacrocycle $Ir_2(CO)_2Cl_2\{\mu\text{-}(Ph_2PCH_2)_2AsPh\}_2$

Alan L. Balch,* Vincent J. Catalano, Mark A. Chatfield, Jeffrey K. Nagle, Marilyn M. Olmstead, and Phillip E. Reedy, Jr.

Contribution from the Department of Chemistry, University of California, Davis, California 95616. *Received July 30, 1990*

Abstract: The ability of the metallomacrocycle $Ir_2(CO)_2Cl_2(\mu\text{-dpma})_2$ (**1**; dpma is bis(diphenylphosphinomethyl)phenylarsine) to coordinate a variety of main-group ions (Pb(II), Sn(II), Ge(II), Tl(I), In(I), Sb(III), Bi(III)) with an s^2 electron configuration is surveyed. Reaction of **1** with sodium iodide, lead(II) iodide, and ammonium hexafluorophosphate yields magenta $[Ir_2(PbI)(CO)_2I_2(\mu\text{-dpma})_2](PF_6)\cdot CH_2Cl_2$, which crystallizes in the triclinic space group $P\bar{1}$ (No. 2) with a = 15.963 (6) Å, b = 16.146 (6) Å, c = 16.869 (9) Å, α = 95.68 (1)°, β = 104.49 (1)°, γ = 117.83 (1)° at 130 K and Z = 2. Refinement of 8994 reflections with 456 parameters yielded R = 0.059, R_w = 0.057. The structure of the cation consists of a PbI unit suspended at the center of the metallomacrocycle through two Pb–Ir bonds (Pb–Ir distances, 2.855 (2), 2.831 (2) Å), which are shorter than the Pb–I bond (2.892 (2) Å). Antimony(III) fluoride and sodium tetrafluoroborate react with **1** to yield $[Ir_2(SbF_2)(CO)_2Cl_2(\mu\text{-dpma})_2](BF_4)$, which crystallizes in the orthorhombic space group *Pmnb* (No. 62) with a = 19.800 (5) Å, b = 19.832 (4) Å, c = 19.865 (4) Å at 130 K with Z = 4. Refinement of 3789 reflections and 233 parameters yielded R = 0.083, R_w = 0.070. The structure consists of the cation, which has crystallographic mirror symmetry, with an SbF_2^+ unit (that lies in the mirror plane) bound to two iridium atoms with two equivalent Sb–Ir distances of 2.655 (1) Å. The arrangement of the two dpma ligands in the macrocycle differs from other adducts because the relative orientation of the lone pairs on the arsenic atoms is trans (i.e., they lie on opposite sides of the rough P_4Ir_2 plane). This implies either inversion of the configuration at arsenic or dissociation of a dpma ligand during formation of the cationic complex. Spectroscopic features of these adducts are compared to those of related complexes with Tl^+ and $(SnCl)^+$ bound to the center of the metallomacrocycle. All show intense absorption in the visible spectrum and luminescence from solutions.

Introduction

A number of recent studies have revealed the ability of main-group metal ions with an s^2 electronic configuration (for example Tl(I)) to participate in bonding to transition metals[1-7] in a fashion that appears analogous to the self-association of uncrowded planar d^8 complexes[8] and to the ubiquitous gold–gold interactions seen in so many two-coordinate complexes of gold(I).[9] Relativistic effects are believed to play an important role (by contracting the s (and p) orbitals and expanding the d orbitals) in promoting metal–metal bonding in complexes with the heavy metals.[10]

The metallomacrocycle **1** is particularly adept at binding such main-group ions (M^{n+}).[11] The flexible cyclic structure, coupled

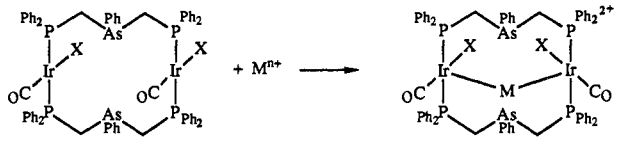

1 X = Cl, Br, or I

with the availability of two d^8 iridium ions that are suitably positioned for chelation, gives this complex a unique propensity to bind a variety of metal ions. The arsenic atoms provide binding sites that facilitate binding of transition-metal ions,[12-14] while the iridium ions are the major binding sites when main-group ions are coordinated.[1,5] This research group has previously described in detail the physical and chemical properties of a complex of **1** with tin(II)[5] and briefly reported on the thallium(I) and lead(II) complexes.[1] These complexes are intensely colored and show strong photoluminescence. Here we survey the ability of **1** to bind to main-group ions that are isoelectronic with Sn(II) and Tl(I).

Results

Group 14. Lead(II). Treatment of a yellow dichloromethane solution of $Ir_2(CO)_2I_2(\mu\text{-dpma})_2$ with lead(II) iodide and ammonium hexafluorophosphate gives a magenta solution from which $[Ir_2(PbI)(CO)_2I_2(\mu\text{-dpma})_2](PF_6)$ may be isolated as red crystals through the addition of ammonium hexafluorophosphate and concentration. Similarly, addition of a slurry of lead(II) nitrate in a water/methanol mixture to a solution of $Ir_2(CO)_2X_2(\mu\text{-dpma})_2$ (X = Cl, Br, I) in dichloromethane results in a color change from yellow to red. The salts, $[Ir_2(PbNO_3)(CO)_2X_2(\mu\text{-dpma})_2](NO_3)$, can be isolated by the addition of more methanol. The electrical conductivity in dichloromethane solution indicates that $[Ir_2(PbNO_3)(CO)_2Cl_2(\mu\text{-dpma})_2](NO_3)$ is a 1:1 electrolyte. Spectroscopic data for these and other adducts of **1** are given in Table I. The electronic absorption spectrum for $[Ir_2(PbI)(CO)_2I_2(\mu\text{-dpma})_2](PF_6)$ is shown in trace A of Figure 1. It is dominated by an intense band at 576 nm. The emission spectrum recorded from a dichloromethane solution at 23 °C with irradiation at 576 nm is shown in trace B. An intense emission is observed at λ_{max} = 594 nm, while a small band appears at 833 nm. When the sample is frozen at −196 °C, the emission spectrum shows no major

(1) Balch, A. L.; Nagle, J. K.; Olmstead, M. M.; Reedy, P. E., Jr. *J. Am. Chem. Soc.* **1987**, *109*, 4123.
(2) Nagle, J. K.; Balch, A. L.; Olmstead, M. M. *J. Am. Chem. Soc.* **1988**, *110*, 319. Ziegler, T.; Nagle, J. K.; Snijders, J. G.; Baerends, E. J. *J. Am. Chem. Soc.* **1989**, *111*, 5631.
(3) Wang, S.; Fackler, J. P., Jr.; King, C.; Wang, J. C. *J. Am. Chem. Soc.* **1988**, *110*, 3308.
(4) Wang, S.; Garzōn, G.; King, C.; Wang, J.-C.; Fackler, J. P., Jr. *Inorg. Chem.* **1989**, *28*, 4623.
(5) Balch, A. L.; Olmstead, M. M.; Oram, D. E.; Reedy, P. E., Jr.; Reimer, S. H. *J. Am. Chem. Soc.* **1989**, *111*, 4021.
(6) Balch, A. L.; Rowley, S. P. *J. Am. Chem. Soc.* **1990**, *112*, 6139.
(7) Balch, A. L.; Davis, B. J.; Olmstead, M. M. *Inorg. Chem.* **1990**, *29*, 3066.
(8) Gliemann, G.; Yersin, H. *Struct. Bonding* **1985**, *62*, 87. Williams, J. *Adv. Inorg. Chem. Radiochem.* **1983**, *26*, 235. Mann, K. R.; Lewis, N. S.; Williams, R. M.; Gray, H. B.; Gordon, J. G., II *Inorg. Chem.* **1978**, *17*, 828.
(9) Jones, P. G. *Gold. Bull.* **1981**, *14*, 102; **1981**, *14*, 159; **1983**, *16*, 114; **1986**, *19*, 46. Schmidbaur, H.; Graf, W.; Müller, G. *Agnew. Chem., Int. Ed. Engl.* **1988**, *27*, 417. Schmidbaur, H. *Gold. Bull.* **1990**, *23*, 11. Jiang, Y.; Alvarez, S.; Hoffmann, R. *Inorg. Chem.* **1985**, *24*, 749. King, C.; Wang, J.-C.; Khan, Md. N. I.; Fackler, J. P., Jr. *Inorg. Chem.* **1989**, *28*, 2145.
(10) Pyykkö, P.; Desclaux, J. P. *Acc. Chem. Res.* **1979**, *12*, 276. Pitzer, K. *Acc. Chem. Res.* **1979**, *12*, 271. Pyykkö, P. *Chem. Rev.* **1988**, *88*, 563.
(11) Balch, A. L. *Pure Appl. Chem.* **1988**, *60*, 555.
(12) Balch, A. L.; Fossett, L. A.; Olmstead, M. M.; Oram, D. E.; Reedy, P. E., Jr. *J. Am. Chem. Soc.* **1985**, *107*, 5272.
(13) Balch, A. L.; Nagle, J. K.; Oram, D. E.; Reedy, P. E., Jr. *J. Am. Chem. Soc.* **1988**, *110*, 454.
(14) Balch, A. L.; Ghedini, M.; Oram, D. E.; Reedy, P. E., Jr. *Inorg. Chem.* **1987**, *26*, 1223.

0002-7863/91/1513-1252$02.50/0

Table I. Spectroscopic Data

compound	UV-vis absorptn,[a] λ_{max}, nm (ϵ, M^{-1} cm^{-1})	emissn,[a] λ_{max}, nm	IR ν(CO),[b] cm^{-1}	$^{31}P\{^1H\}$NMR,[c] δ (ppm)
$[Ir_2(PbI)(CO)_2I_2(\mu\text{-dpma})_2](PF_6)$	576 (59000), 448 (6000), 350 (13000)	620, 833	1975	16.85
$[Ir_2(PbNO_3)(CO)_2Cl_2(\mu\text{-dpma})_2](NO_3)$	538 (62000), 388 (4800), 326 (11000)	563, 825	1978, 1984	24.4
$[Ir_2(PbNO_3)(CO)_2Br_2(\mu\text{-dpma})_2](NO_3)$	548 (63000), 422 (5700), 330 (13000)	585, 830	1977	21.6
$[Ir_2(PbNO_3)(CO)_2I_2(\mu\text{-dpma})_2](NO_3)$	574 (64000), 446 (9000), 348 (16000)	612, 832	1975	16.8
$[Ir_2(SnCl)(CO)_2Cl_2(\mu\text{-dpma})_2](SnCl_3)$	588 (77000), 450 (5200), 399 (4900)	645	1987, 1974	26.9
$Ir_2(TlNO_3)(CO)_2Cl_2(\mu\text{-dpma})_2$	516 (33000), 380 (12000)	580, 814	1973	20.6
$Ir_2(TlNO_3)(CO)_2Br_2(\mu\text{-dpma})_2$	550 (32000), 382 (10000)	606, 825	1969	16.2
$Ir_2(TlNO_3)(CO)_2I_2(\mu\text{-dpma})_2$	563 (37000), 394 (7700)	630, 830	1967	10.7
$[Ir_2(SbF_2)(CO)_2Cl_2(\mu\text{-dpma})_2](PF_6)$	538 (100000)	581, 840	2019	21.6, 29.9[d]

[a] In dichloromethane solution. [b] Nujol mull. [c] In dichloromethane-d_2 solution. [d] AB quartet with J(P,P) = 300 Hz.

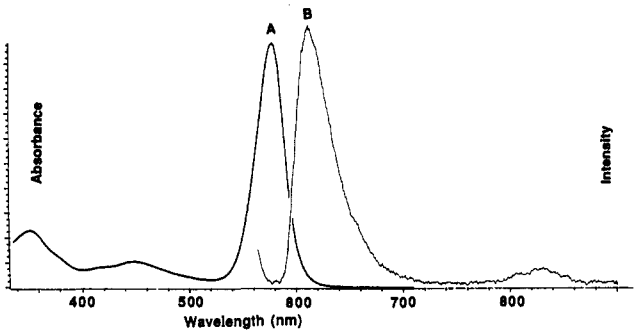

Figure 1. Electronic absorption (A) and uncorrected emission (B) spectra of $[Ir_2(PbI)(CO)_2I_2(\mu\text{-dpma})_2](PF_6)$ in dichloromethane at 23 °C.

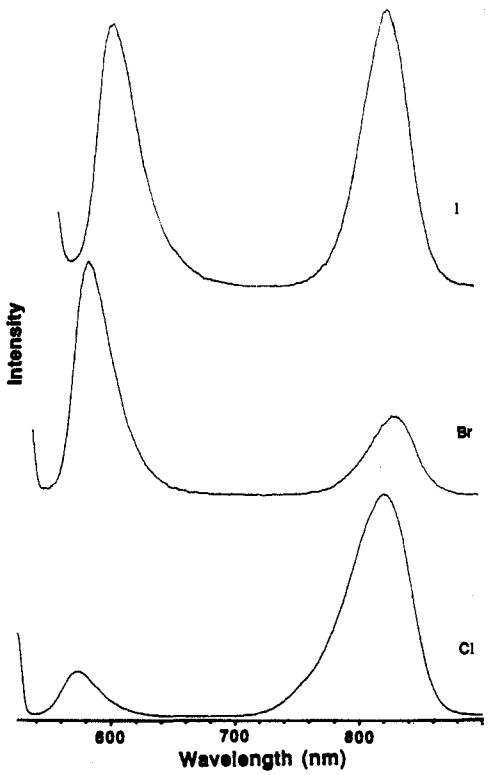

Figure 2. Uncorrected emission spectra for Cl, $[Ir_2(PbNO_3)(CO)_2Cl_2(\mu\text{-dpma})_2](NO_3)$; Br, $[Ir_2(PbNO_3)(CO)_2Br_2(\mu\text{-dpma})_2](NO_3)$; and I, $[Ir_2(PbNO_3)(CO)_2I_2(\mu\text{-dpma})_2](NO_3)$ in dichloromethane at 23 °C.

change. The salts $[Ir_2(PbNO_3)(CO)_2X_2(\mu\text{-dpma})_2](NO_3)$ produce similar absorption spectra. These show shifts of the prominent absorption band to lower energy as the halide ligands on iridium are changed from chloride to bromide and then to iodide. Their emission spectra exhibit two emissions as seen in Figure 2. Notice that the relative intensities of the two emissions vary greatly as the halide ligands are altered. The emission lifetimes have been recorded for $[Ir_2(PbNO_3)(CO)_2Cl_2(\mu\text{-dpma})_2](NO_3)$. For the low-energy emission in dichloromethane solution at 23 °C, the lifetime is 1.4 μs while it is less than 50 ns for the high-energy emission. On the basis of the relatively long lifetime and the large Stokes' shift, the low-energy emission of $[Ir_2(PbNO_3)(CO)_2Cl_2(\mu\text{-dpma})_2](NO_3)$ is assigned to phosphorescence, while the high-energy emission, which is nearly the mirror image of the absorption, is assigned to fluorescence. The infrared spectra of these adducts show ν(CO) in the range 1984–1975 cm^{-1}, which is consistent with observations on other iridium(I) complexes. The $^{31}P\{^1H\}$ NMR spectra show a single resonance for each cation. This is expected for adducts in which the lead is symmetrically bonded to both iridium atoms and all four phosphorus atoms are equivalent.

Table II. Selected Interatomic Distances and Angles for $[Ir_2(PbI)(CO)_2I_2(\mu\text{-dpma})_2](PF_6)\cdot CH_2Cl_2$

Distances, Å			
at Ir(I)			
Ir(1)–Pb	2.855 (2)	Ir(1)–I(1)	2.646 (2)
Ir(1)–P(1)	2.334 (5)	Ir(1)–C(1)	1.79 (2)
Ir(1)–P(4)	2.331 (6)		
at Pb			
Pb–Ir(1)	2.855 (2)	Pb···As(1)	3.141 (3)
Pb–Ir(2)	2.831 (2)	Pb···As(2)	3.185 (3)
Pb–I(3)	2.892 (2)		
at Ir(2)			
Ir(2)–Pb	2.831 (2)	Ir(2)–I(2)	2.645 (2)
Ir(2)–P(2)	2.342 (5)	Ir(2)–C(2)	1.85 (1)
Ir(2)–P(3)	2.335 (6)		
Angles, deg			
at Ir(1)			
P(4)–Ir(1)–P(1)	166.2 (1)	Pb–Ir(1)–C(1)	100.6 (5)
I(1)–Ir(1)–C(1)	169.7 (5)	P(4)–Ir(1)–I(1)	86.5 (1)
Pb–Ir(1)–P(4)	95.6 (1)	P(4)–Ir(1)–C(1)	92.5 (7)
Pb–Ir(1)–P(1)	96.2 (1)	P(1)–Ir(1)–I(1)	86.3 (1)
Pb–Ir(1)–I(1)	89.7 (1)	P(1)–Ir(1)–C(1)	92.4 (7)
at Ir(2)			
P(2)–Ir(2)–P(3)	165.3 (2)	Pb–Ir(2)–C(2)	99.0 (5)
I(2)–Ir(2)–C(2)	169.9 (5)	P(2)–Ir(2)–I(2)	86.6 (1)
Pb–Ir(2)–P(2)	96.3 (1)	P(2)–Ir(2)–C(2)	91.7 (6)
Pb–Ir(2)–P(3)	96.7 (1)	P(3)–Ir(2)–I(2)	86.2 (1)
Pb–Ir(2)–I(2)	91.0 (1)	P(3)–Ir(2)–C(3)	93.1 (6)
at Pb			
Ir(1)–Pb–Ir(2)	146.4 (1)	Ir(2)–Pb–As(1)	87.8 (1)
Ir(1)–Pb–I(3)	108.6 (1)	Ir(2)–Pb–As(2)	87.2 (1)
Ir(2)–Pb–I(3)	105.0 (1)	I(3)–Pb–As(1)	97.5 (1)
Ir(1)–Pb–As(1)	87.3 (1)	I(3)–Pb–As(2)	99.0 (1)
Ir(1)–Pb–As(2)	88.2 (1)		

The Structure of $[Ir_2(PbI)(CO)_2I_2(\mu\text{-dpma})_2](PF_6)\cdot CH_2Cl_2$. The asymmetric unit contains the cation, a normal hexafluorophosphate, and a dichloromethane molecule with no unusual contacts between these units. Figure 3 shows a drawing of the cation. Selected interatomic distances and angles are given in Table II. Although the cation does not have crystallographically imposed symmetry, it does approximate C_{2v} symmetry with the 2-fold axis running along the Pb–I bond.

The cation consists of the intact metallomacrocycle with a PbI unit suspended symmetrically between the two iridium ions. The $IrP_2(CO)I$ unit retains its basic trans planar geometry, but the P–Ir–P units are bent slightly inward so that the iridium ions can

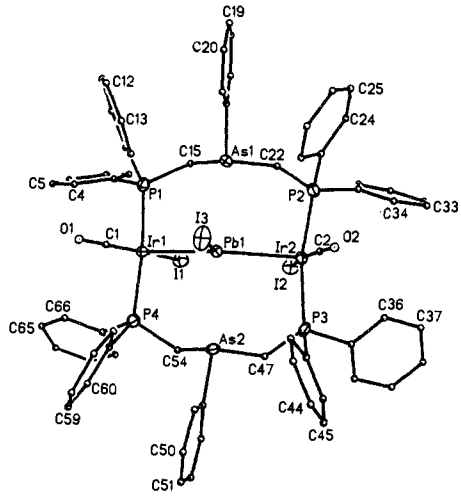

Figure 3. Perspective drawing of the cation in $[Ir_2(PbI)(CO)_2I_2(\mu\text{-dpma})_2](PF_6)$ using 50% thermal contours for the heavy atoms and uniform, arbitrarily sized circles for carbon atoms.

approach the lead ion. As is typical with such complexes, the halide ligands (iodide) are both located on the face opposite the added metal (PbI unit). The Pb–Ir distances, 2.855 (2) and 2.831 (2) Å, are nearly equal and are *shorter* than the Pb–I distance, 2.892 (2) Å. In comparison, the Pb–I distances in the PbI_6 octahedra in $KPbI_3{\cdot}2H_2O$ range from 3.032 (1) to 3.461 (1) Å.[15] This difference may reflect the high coordination number for lead in $KPbI_3{\cdot}2H_2O$. The Ir–Pb–Ir unit is bent (166.2 (1)°), and the two Ir–Pb–I angles are similar (108.6 (1)°, 105.0 (1)°). The Ir_2PbI unit is planar; the sum of the Ir–Pb–Ir and the two Ir–Pb–I angles is 360°. The Pb···As distances are rather long (3.141 (3), 3.185 (3) Å). These are clearly longer than the sum of the covalent radius for arsenic (1.20 Å) and the covalent radius for lead(II) (1.47 Å)[16] and exceed by ~0.1 Å the longest Pb–As distances predicted by comparison to $Pb\{(Ph_2P)_2CSiMe_3\}_2$.[17,18] Another way of viewing the bonding is to examine the bond angles about arsenic. When the hypothetical position of the arsenic lone pair is computed by placing it equidistant from the three As–C bonds, the angles between the Pb–As line and the position of the arsenic lone pair are 30.1° for As(I) and 34.8° for As(2). Figure 4 shows a side view of the inner coordination of $[Ir_2(PbI)(CO)_2I_2(\mu\text{-dpma})_2]^+$, which emphasizes the angular distribution of groups about arsenic and their relation to the location of the lead ion. It is clear that the two arsenic atoms are not optimally located for bonding to lead and that the strength of the Pb···As interaction is insufficient to reorient the arsenic atoms in the fashion seen for corresponding transition-metal complexes containing the same ligand system. Figure 4 shows a similar view of $[Ir_2Au(CO)_2Cl_2(\mu\text{-dpma})_2]^+$[13] where the angles between the hypothetical lone-pair position on the As–Au lines are only 7.2 and 8.9°, and the distances are much shorter (2.397 (1) Å for both).

Tin(II). The tin(II) adduct $[Ir_2(SnCl)(CO)_2Cl_2(\mu\text{-dpma})_2]^+$ has been discussed in detail previously.[5] For comparison, spectral properties are given in Table I. The electronic spectrum is dominated by an absorption at 588 nm, while the emission spectrum shows only a single band at 645 nm at 23 °C in dichloromethane. Freezing the sample at −196 °C produces only minor changes in the emission spectrum. In particular, there is no evidence for a second, lower energy emission.

Germanium(II). Treatment of a dichloromethane solution of $Ir_2(CO)_2I_2(\mu\text{-dpma})_2$ with germanium(II) iodide produces an intensely blue solution, but the adduct responsible for the color has not been isolated. These solutions have a strong absorption at 556 nm with emissions at 636 and 820 nm at 23 °C. The $^{31}P\{^1H\}$ NMR spectrum reveals, however, three new peaks at 18.7, 14.2, and −24.3 ppm along with a major resonance (at 12.4 ppm) due to unreacted $Ir_2(CO)_2I_2(\mu\text{-dpma})_2$. Although it is likely that the major colored and emitting species is analogous to the well-characterized lead(II) and tin(II) adducts, further study of the mixture of products was obviated by the low conversion and the inability to isolate a single pure component from the mixture. The reaction between **1** and $GeCl_2{\cdot}2$(dioxane) gave similar results.

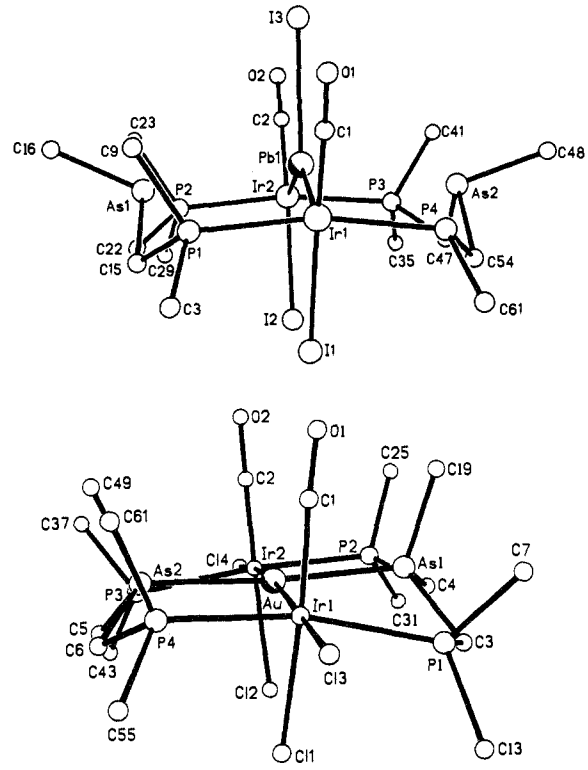

Figure 4. Views of the inner coordination of (top) $[Ir_2(PbI)(CO)_2I_2(\mu\text{-dpma})_2]^+$ and (bottom) $[Ir_2Au(CO)_2Cl_2(\mu\text{-dpma})_2]^+$.

Group 13. Thallium(I). Treatment of dichloromethane solutions of $Ir_2(CO)_2X_2(\mu\text{-dpma})_2$ with thallium(I) nitrate in methanol produces red-orange solutions from which the adducts $Ir_2(TlNO_3)(CO)_2X_2(\mu\text{-dpma})_2$ can be precipitated by the addition of more methanol. The conductivity of $Ir_2(TlNO_3)(CO)_2X_2(\mu\text{-dpma})_2$ in dichloromethane solution indicates that there is little dissociation occurring, and hence the nitrate ion remains coordinated to the thallium. Spectroscopic data for three adducts with X = Cl, Br, and I are given in Table I. The electronic absorption spectra are dominated by intense features at ca. 500–550 nm (see Figure 1 of ref 1). As with the lead(II) complexes, changing the halide ligands on iridium from chloride to bromide and to iodide results in lowering of the energy of the prominent absorption band. The emission spectra of all three show two emissions as shown in Figure 5. Unlike the case with the lead(II) adducts (Figure 2), all three show similar relative intensities for the two emissions. In dichloromethane solution at 23 °C, the lifetime of the low-energy emission is 1.4 μs while that of the high-energy emission is less the 50 ns. As with the lead adducts these can be assigned as phosphorescence (low energy) and fluorescence (high energy).

The structure of the thallium(I) adduct, $Ir(TlNO_3)(CO)_2Cl_2(\mu\text{-dpma})_2$, has been described earlier.[1] The structure is similar to that of $[Ir(PbI)(CO)_2I_2(\mu\text{-dpma})]^+$ with a thallium ion replacing the lead and a bidentate nitrate replacing the iodide. Comparative data for various adducts of **1** are given in Table III.

Indium(I). Addition of solid indium(I) chloride to a oxygen-free dichloromethane solution of **1** produces a green solution (λ_{max} = 626 nm) with emission at 704 nm. This fades in a matter of tens of minutes to give an orange, nonemitting solution. Although the

(15) Bedlivy, D.; Mereiter, K. *Acta Crystallogr.* **1980**, *36B*, 782.
(16) Greenwood, N. N.; Earnshaw, A. *Chemistry of the Elements*; Pergamon Press: Oxford, 1984; pp 431, 643.
(17) No simple covalent complexes containing Pb–As bonds appear to have been structurally characterized. $Pb\{(Ph_2P)_2CSiMe_3\}_2$, with Pb–P bond lengths ranging from 2.72 to 2.97 Å, is a rare example of a compound with Pb–P bonds. In general, bonds to arsenic are 0.1 Å longer than similar bonds involving phosphorus.
(18) Balch, A. L.; Oram, D. E. *Inorg. Chem.* **1987**, *26*, 1906.

Table III. Comparison of Structural Parameters for Adducts of $Ir_2(CO)_2X_2(\mu\text{-dpma})_2$ (**1**)

compound	M–Ir distance, Å	Ir–M–Ir angle, deg	As···M distance, Å	Ir···Ir distance, Å	M···As/lone pair angle,[a] deg	ref
$[Ir_2(PbI)(CO)_2I_2(\mu\text{-dpma})_2]^+$	2.855 (2)	146.4 (1)	3.141 (3)	5.443 (2)	30	this work
	2.831 (2)		3.185 (3)		34	
$[Ir_2(SnCl)(CO)_2Cl_2(\mu\text{-dpma})_2]^+$	2.741 (2)	146.1 (1)	3.173 (5)	5.245 (2)	36	5
	2.742 (2)		3.062 (5)		32	
$Ir_2(TlNO_3)(CO)_2Cl_2(\mu\text{-dpma})_2$	2.958 (1)	139.4 (1)	3.295 (3)	5.569 (1)	38	1
	2.979 (1)		3.308 (3)		41	
$[Ir_2(SbF_2)(CO)_2Cl_2(\mu\text{-dpma})_2]^+$	2.655 (1)	157.5 (1)	3.514 (8)	5.208 (1)	52	this work
			3.032 (8)		36	
$[Ir_2(Au)(CO)_2Cl(\mu\text{-dpma})_2]^+$	3.059 (1)	149.0 (1)	2.397 (1)	5.850 (1)	7	13
	3.012 (1)		2.397 (1)		9	
$[Ir_2(Au)(CO)_2Cl_4(\mu\text{-dpma})_2]^+$	2.812 (2)	173.1 (1)	2.379 (4)	5.608 (2)	3	13
	2.806 (2)		2.386 (4)		6	
$Ir_2(AgCl)(CO)_2Cl_2(\mu\text{-dpma})_2$	3.362 (2)	131.5 (1)	2.558 (4)	6.125 (2)	7	5
	3.356 (2)		2.585 (4)		3	

[a] Angle between the M···As line and the As lone-pair position computed from the location of the three carbon atoms bound to arsenic.

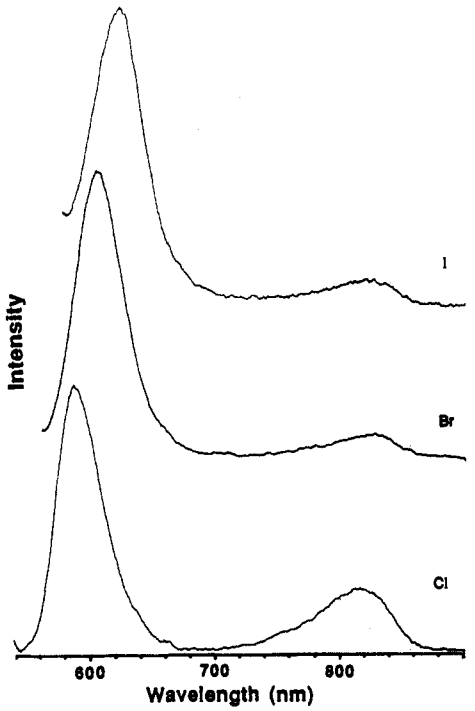

Figure 5. Uncorrected emission spectra for Cl, $Ir_2(TlNO_3)(CO)_2Cl_2(\mu\text{-dpma})_2$; Br, $Ir_2(TlNO_3)(CO)_2Br_2(\mu\text{-dpma})_2$; and I, $Ir_2(TlNO_3)(CO)_2I_2(\mu\text{-dpma})_2$ in dichloromethane at 23 °C.

green species is probably analogous to the thallium(I) adduct, thorough characterization was hampered by the intrinsic instability of the adduct.

Group 15. Antimony(III). Reaction of **1** with solid antimony(III) fluoride in dichloromethane produces a pink solution, which yields solid $[Ir_2(SbF_2)(CO)_2Cl_2(\mu\text{-dpma})_2](BF_4)$ after treatment with sodium tetrafluoroborate. The electronic absorption (trace A) and emission (trace B) spectra are shown in Figure 6. The absorption spectrum shows an intense feature at 538 nm while the emission spectrum consists of a peak at 590 nm and a weaker emission at 840 nm. Freezing the sample at 77 K shifts the emission maximum of the higher energy band to 604 nm, but otherwise does not alter the spectrum.

The $^{31}P\{^1H\}$ NMR spectrum consists of an AB quartet with δ_1 = 21.6 ppm, δ_2 = 29.9 ppm, and $J(P_A,P_B)$ = 300 Hz. This pattern is consistent with a structure in which the two dpma ligands are inequivalent but remain trans to one another (i.e., $J(P_A,P_B)$ is consistent with a trans P_AIrP_B arrangement). Further coupling to another spin $^1/_2$ nucleus (presumably fluoride) is seen. Thus, the resonances at 21.6 ppm show further doublet splitting with $J(P,F)$ = 12 Hz, while the resonances at 29.9 ppm also show doublet splitting with $J(P,F)$ = 9 Hz. The structure (vide infra) shows that one Sb–F bond (that involving F(1)) is nearly perpendicular to the P–Ir–P units. The Karplus relationship for coupling constants suggests that coupling to that fluoride will be small, and it is indeed not observed, while coupling to F(2) is responsible for the observed doublets. The ^{19}F NMR spectrum showed resonances at −72.8 and −19.5 ppm due to the SbF_2 group. The spectral resolution was not sufficient to observe the P–F coupling, nor was any F–F coupling observed.

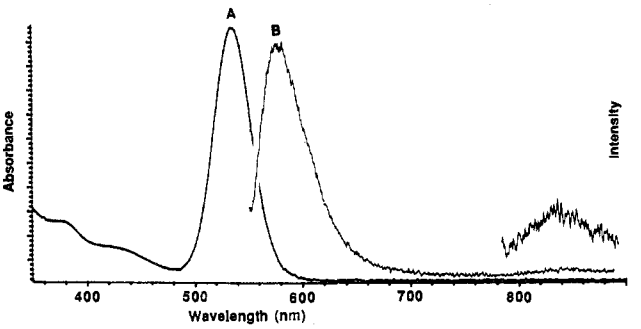

Figure 6. Electronic absorption (A) and uncorrected emission (B) spectra of $[Ir_2(SbF_2)(CO)_2Cl_2(\mu\text{-dpma})_2](BF_4)$ in dichloromethane at 23 °C.

Table IV. Selected Interatomic Distances and Angles for $[Ir_2(SbF_2)(CO)_2Cl_2(\mu\text{-dpma})_2](BF_4)$

	Distances, Å		
	at Ir		
Ir–Sb	2.655 (1)	Ir–Cl	2.358 (6)
Ir–P(1)	2.334 (6)	Ir–C(1)	1.82 (2)
Ir–P(2)	2.364 (6)		
	at Sb		
Sb–Ir	2.655 (1)	Sb···As(1)	3.514 (8)
Sb–F(1)	1.95 (2)	Sb···As(2)	3.032 (8)
Sb–F(2)	1.98 (2)		
	Angles, deg		
	at Ir		
P(1)–Ir–P(2)	161.2 (2)	P(1)–Ir–Cl	84.1 (2)
Cl–Ir–C(1)	174.3 (8)	P(1)–Ir–C(1)	94.7 (8)
Sb–Ir–P(1)	97.4 (2)	P(2)–Ir–Cl	86.0 (2)
Sb–Ir–P(2)	98.8 (2)	P(2)–Ir–C(1)	93.5 (8)
Sb–Ir–Cl	91.8 (2)	Ir(1)–C(1)–O(1)	174 (2)
Sb–Ir–C(1)	93.8 (8)		
	at Sb		
Ir–Sb–Ir′	157.5 (1)	Ir–Sb–F(1)	100.2 (1)
F(1)–Sb–F(2)	83.7 (8)	Ir–Sb–F(2)	95.9 (1)

The infrared spectrum shows ν(CO) at 2019 cm^{-1}, which is a sizable increase over that of **1**, particularly when it is compared to that of the other adducts in Table I. Clearly, binding of the SbF_2^+ group produces a significant drain of electron density at the iridium centers and a reduction in back-bonding to the adjacent carbon monoxide ligands.

The Structure of $[Ir_2(\mu\text{-}SbF_2)(CO)_2Cl_2(\mu\text{-dpma})_2](BF_4)$. The asymmetric unit contains half of the cation, which has mirror

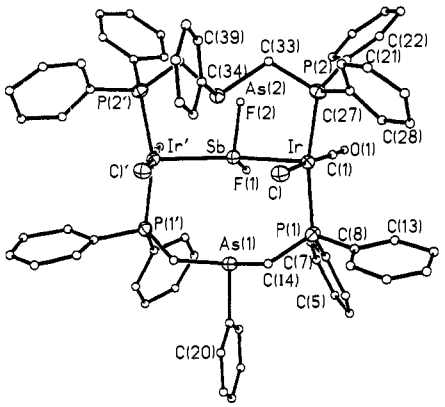

Figure 7. Drawing of the cation in $[Ir_2(SbF_2)(CO)_2Cl_2(\mu\text{-dpma})_2](BF_4)$.

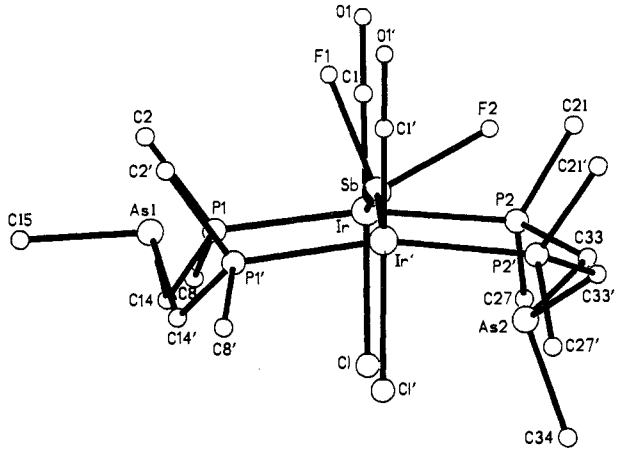

Figure 8. View of the inner coordination core of $[Ir_2(SbF_2)(CO)_2Cl_2(\mu\text{-dpma})_2]^+$.

symmetry, and half of a bulky disordered fluoroborate ion in the asymmetric unit. The structure of the cation is shown in Figure 7. Selected interatomic distances are given in Table IV.

The cation contains a SbF_2^+ unit, which bridges the two *trans*-$P_2Ir(CO)Cl$ units. The SbF_2 unit lies in the mirror plane and the Sb–Ir distances (2.655 (1) Å) are required by symmetry to be equivalent. They also are shorter than the other iridium–main-group ion distances in the other metallomacrocyclic complexes in this series (see Table III). As is usual for these complexes, the Ir–Sb–Ir angle (157.5 (1)°) is bent. The Sb–F distances (1.95 (2), 1.98 (2) Å) and the F–Sb–F angle (183.7 (8)°) are unremarkable.[19] The $\{Ir(CO)Cl\}_2Sb$ unit is nearly planar. The largest out-of-plane displacement is 0.005 Å for Ir.

The orientation of the two dpma ligands is quite remarkable. This is best appreciated by inspecting Figure 8. One arsenic and its lone pair reside on one side of the mean P_4Ir_2 plane while the other arsenic atom and its lone pair reside on the opposite side. Contrastingly, in the other complexes of **1**, the two arsenic atoms reside on the same side of the mean P_4Ir_2 plane, and their lone pairs are directed toward the same side of that plane. This can be seen for $[Ir_2(PbI)(CO)_2I_2(\mu\text{-dpma})_2]^+$ and $[Ir_2Au(CO)_2Cl_2(\mu\text{-dpma})_2]^+$ in Figure 4. The relative orientations of the PhAs groups in $Rh_2(CO)_2Cl_2(\mu\text{-dpma})_2$ (which we believe is very similar to **1**) have been described in detail.[14] In it, the relative orientations of the PhAs groups are such that simple inward folding will place them in the positions seen for $[Ir_2(PbI)(CO)_2Cl_2(\mu\text{-dpma})_2]^+$ and $[Ir_2Au(CO)_2Cl_2(\mu\text{-dpma})_2]^+$. In order to get the relative orientations seen in $[Ir_2(SbF_2)(CO)_2Cl_2(\mu\text{-dpma})_2]^+$, either one of the arsenic atoms undergoes inversion or an entire dpma ligand dissociates at the two P–Ir bonds. When a dpma reattaches itself it does so such that the altered geometry is obtained. Barriers for inversion at arsenic are high (ca. 42 kcal/mol).[21] Consequently, unless somehow catalyzed, inversion is unlikely. On the other hand, we have recently encountered a number of reactions in which Ir–P bond breaking must occur during the formation of polynuclear species.[20] Consequently we suspect that Ir–P bond breaking has occurred during the formation of the SbF_2^+ adduct. The two different Sb···As distances are long, 3.032 (8) and 3.514 (8) Å, and the arsenic lone pairs lie 52.3° (for As(1)) and 35.7° (for As(2)) away from lines connecting antimony and arsenic. These pronounced differences, which are unlike the symmetrical arrangements seen for the lead, tin, and thallium adducts, reflect the two different orientations of the dpma ligands in the SbF_2^+ adduct.

Bismuth(III). Treatment of an acetone solution **1** with bismuth(III) nitrate yields a red solution with absorption at 534 nm and emissions at 570 and 820 nm. The ^{31}P NMR spectrum shows that a mixture of phosphorus-containing species is formed. An effective method of separating these has not been found.

Discussion

Four adducts of the metallomacrocycle **1** that involve complexing of main-group ions have now been isolated and characterized by X-ray crystallography (see Table III). In each case the main-group ion coordinates to iridium in preference to arsenic, and the Ir–M–Ir unit is bent. The bond distances involved increase in the order Sb–Ir < Sn–Ir ~ Pb–Ir < Tl–Ir. The facts that the Sb–Ir bonds are shorter than the Sn–Ir bonds and that the Pb–Ir bonds are shorter than the Tl–Ir bonds follow the usual trend based on oxidation state. Thus, for example, Pb(II) is expected to have a smaller radius than Tl(I). Within this series there is also a correlation between M–Ir bond lengths and the Ir–M–Ir angles. As the M–Ir bonds shorten, the Ir–M–Ir angles increase. Likewise, as the M–Ir bond lengths contract, the nonbonded Ir···Ir separations decrease. However, bending at M modulates this somewhat, so that the Ir···Ir separations differ by a maximum of 0.36 Å for the four adducts. In the cases of these four main-group ions, bonding to arsenic, if present at all, is insufficient to reorient the arsenic lone pairs so that maximal overlap with the central metal would be achieved. The M···As distances are in all four cases over 0.6 Å longer than the M–As bond distances seen in the cases where comparably sized transition-metal ions are bound to **1**.

Of the metal ions considered here, only tin(II) shows a strong proclivity to bind transition-metal ions. Indeed, numerous complexes involving the $SnCl_3^-$ group, particularly bound to the platinum group metals, are known.[22,23] In contrast, efforts to make analogous complexes with lead (with a $PbCl_3^-$ group) have been unsuccessful.[23] The unusual polymeric chain in $\{Au_2Pb(CH_2P(S)Ph_2)_2\}$ offers a rare example of transition metal/lead bonding.[4] The Au–Pb distances (2.896 (1), 2.963 (2) Å) in this compound[4] are just slightly longer than the Ir–Pb distances in $[Ir_2(PbI)(CO)_2I_2(\mu\text{-dpma})_2]^+$.

The bonding in these adducts can be viewed in terms of the models previously developed for the thallium[1] and tin[5] adducts. This involves overlap of the filled out-of-plane d_{z^2} orbitals on iridium with the filled s orbital on the central metal. This produces the set of filled orbitals labeled $1a_1$, $1b_2$, and $2a_1$ and would yield no net bonding along the Ir–M–Ir chain since the bonding $1a_1$ and antibonding $2a_1$ levels are filled. However, these orbitals will mix with another set of empty orbitals obtained by overlap of the empty p_z orbitals on iridium and on the central main-group ion since there are orbitals of similar symmetry in both sets. It is this mixing of the d and s orbitals with the empty p orbitals that lowers the energy of all of the filled orbitals so that the Ir–M–Ir aggregate is stabilized. This is shown in Figure 9. Thus, the essential electronic features necessary for a main-group ion to bind to **1** are the availability of a filled s orbital and an empty p orbital of suitable energy to match with the iridium orbitals. Consequently

(19) Sawyer, J. F.; Gillespie, R. J. *Prog. Inorg. Chem.* **1986**, *34*, 65.
(20) Balch, A. L.; Catalano, V. J.; Olmstead, M. M. *J. Am. Chem. Soc.* **1990**, *112*, 2010.
(21) Senkler, G. M.; Mislow, K. *J. Am. Chem. Soc.* **1972**, *94*, 291.
(22) Holt, M. S.; Wilson, W. L.; Nelson, J. H. *Chem. Rev.* **1989**, *89*, 11.
(23) Young, J. F.; Gillard, R. D.; Wilkinson, G. *J. Chem. Soc.* **1964**, 5176.

Table V. Crystallographic Data

	$[Ir_2(PbI)(CO)_2I_2(\mu\text{-dpma})_2](PF_6)\cdot CH_2Cl_2$	$[Ir_2(SbF_2)(CO)_2Cl_2(\mu\text{-dpma})_2](BF_4)$
formula	$C_{67}H_{60}O_2P_5Cl_2As_2I_3Ir_2PbF_6$	$C_{66}H_{62}As_2BCl_2F_6Ir_2O_4P_4Sb$
fw	2359.0	1894.87
color and habit	red triangular prisms	red prisms and needles
crystal system	triclinic	orthorhombic
space group	$P\bar{1}$ (No. 2)	*Pmnb* (No. 62)
a, Å	15.963 (6)	19.800 (5)
b, Å	16.146 (6)	19.823 (4)
c, Å	16.869 (9)	19.865 (4)
α, deg	95.68 (1)	
β, deg	104.49 (1)	
γ, deg	117.83 (1)	
V, Å^3	3602 (3)	7797 (3)
T, K	130	130
Z	2	4
cryst dimens, mm	0.25 × 0.25 × 0.58	0.17 × 0.20 × 0.35
d_{calcd}, g cm^{-3}	2.175	1.61
radiation, Å	Mo Kα (λ = 0.71069 Å)	Mo Kα (λ = 0.71069 Å)
μ(Mo Kα), cm^{-1}	84.4	49.9
range of transmission factors	0.63–0.94	0.34–0.50
diffractometer	Siemens R 3m/v	$P2_1$, graphite monochromator
scan method	ω, 1.2° range, 1.0° offset for bdgd	ω, 1.2° range, 4.0° offset for bkgd
scan range, deg	0.0–50.0	0.0–50.0
scan speed, deg min^{-1}	20–58	30
octants collected	$h,k,\pm l$	h,k,l
no. of data collected	12670	7531
no. of unique data	12670	7076 [*R*(merge) = 0.08]
no. of data refined	8994 ($F \geq 4.0\sigma(F)$)	3789 ($I > 2\sigma(I)$)
no. of parameters refined	456	233
R^a	0.059	0.083
$R_w{}^a$	0.057 ($w^{-1} = \sigma^2(F) + 0.0003F^2$)	0.070 ($w = 1/\sigma^2(F_o)$)

$^a R = \sum||F_o| - |F_c||/|F_o|$ and $R_w = \sum||F_o| - |F_c||w^{1/2}/\sum|F_o w^{1/2}|$.

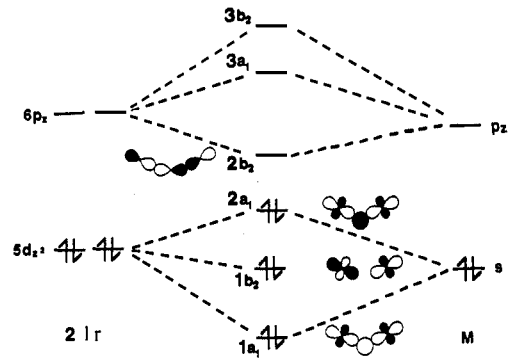

Figure 9. Qualitative molecular orbital diagram for $[Ir_2M(CO)_2Cl_2(\mu\text{-dpma})_2]^{n+}$, focusing on the highest occupied and lowest unoccupied orbitals along the Ir–M–Ir chain.

we find that the set of isoelectronic ions from groups 13, 14, and 15 bind to **1**, but similarly sized ions from groups 1 and 2 (for example, Rb(I), Cs(I), Sr(II), **Ba**(II)), lack the proper electronic characteristics and do not interact with **1**.

These electronic requirements are particularly notable in the reaction of **1** with antimony(III) fluoride. The loss of a fluoride to form the $SbF_2{}^+$ unit is necessary in order to create the vacant p orbital that is required for the bonding model. Notice that the $SbF_2{}^+$ unit is electronically quite distinct from the more conventional stibide ion (R_2Sb^-),[24] as well as the more common phosphides and arsenides, that also function as the bridging groups between metal ions.

These adducts and their analogues with different halide ligands on iridium or different substituents bound to the central main-group ion show intense absorption in the electronic spectrum in the region 530–600 nm and strong emission in solution. The intense absorption feature is believed to result from an allowed transition from the filled $2a_1$ orbital to the empty $2b_2$ level. The lifetimes of the low-energy emissions are in the microsecond range, long enough so that it may be possible to observe chemical reactions of these long-lived excited states. Studies of the photochemical behavior of these and related complexes are in progress. The observation of similar absorption and emission from **1** in the presence of Ge(II), In(I), and Bi(III) suggests that these also form adducts with similar structures, but it has not yet been possible to isolate the adducts involved in pure form.

(24) Barron, A. R.; Cowley, A. M.; Jones, R. A.; Nunn, C. M.; Westmoreland, D. L. *Polyhedron* **1988**, *7*, 77.

Experimental Section

Preparation of Compounds. $Ir_2(CO)_2Cl_2(\mu\text{-dpma})_2$ and its bromo and iodo analogues were prepared as described previously.[12,13]

$[Ir_2(PbNO_3)(CO)_2Cl_2(\mu\text{-dpma})_2](NO_3)$. A slurry of 100 mg (0.30 mmol) of $Pb(NO_3)$ in 0.25 mL of water and 2 mL of methanol was added to a solution of 100 mg (0.062 mmol) of $Ir_2(CO)_2Cl_2(\mu\text{-dpma})_2$ in 4 mL of dichloromethane. The solution immediately turned bright red in color. After it was stirred for 30 min, the solution was filtered to remove unreacted $Pb(NO_3)_2$, and additional methanol was added to precipitate the product as bright pink crystals. The product was collected by filtration and washed with methanol and diethyl ether; yield 90 mg, 75%. Anal. Calcd for $C_{66}H_{58}As_2Cl_2Ir_2N_2O_8P_4Pb$: C, 40.79; H, 3.01; N, 1.44. Found: C, 40.70; H, 3.01; N, 1.45. Conductivity (dichloromethane solution) Λ_m = 47 Ω^{-1} mol^{-1} cm^2.

$Ir_2(TlNO_3)(CO)_2Cl_2(\mu\text{-dpma})_2$. A slurry of 100 mg (0.37 mmol) of $TlNO_3$ in 2 mL of methanol was added to a solution of 100 mg (0.062 mmol) of $Ir_2(CO)_2Cl_2(\mu\text{-dpma})_2$ in 4 mL of dichloromethane. The mixture turned red immediately, and after stirring for 30 min, a brick red precipitate had formed. The solution was filtered to remove unreacted $TlNO_3$ and the precipitated product. The solid was washed with a few milliliters of dichloromethane to dissolve the product, and this solution was filtered to remove the unreacted $TlNO_3$. The two filtrates were then combined, and methanol was added to precipitate the product as red crystals. The product was collected by filtration and washed successively with methanol and diethyl ether; yield 83 mg, 71%. Anal. Calcd for $C_{66}H_{58}As_2Cl_2Ir_2NO_5P_4Tl$: C, 42.19; H, 3.11; N, 0.74; Cl, 3.77. Found: C, 41.61; H, 3.10; N, 0.44; Cl, 3.97. Conductivity (dichloromethane solution) Λ_m = 4 Ω^{-1} mol^{-1} cm^2.

$[Ir_2(PbI)(CO)_2I_2(\mu\text{-dpma})_2](PF_6)$. A slurry of 50 mg (0.33 mmol) of sodium iodide in 0.5 mL of water and 5 mL of methanol was added to a yellow solution containing 100 mg (0.062 mmol) of $Ir_2(CO)_2Cl_2(\mu\text{-dpma})_2$ in 20 mL of dichloromethane. The mixture was stirred for 20 min and filtered through Celite. The volume of the filtrate was reduced under vacuum to form yellow crystals of $Ir_2(CO)_2I_2(\mu\text{-dpma})_2$, which were collected by filtration, washed with ethyl ether, and vacuum dried (yield, 90%). A slurry of 20 mg (0.043 mmol) of lead(II) iodide in 10 mL of methanol was added to a solution of 50 mg (0.028 mmol) of

$Ir_2(CO)_2I_2(\mu\text{-dpma})_2$ in 10 mL of dichloromethane. The deep red solution was stirred for 20 min, and then a solution of 50 mg (0.306 mmol) of ammonium hexafluorophosphate in 20 mL of methanol was added. After the red solution was filtered through Celite, its volume was reduced under vacuum until red crystals formed. These were collected by filtration and washed with ethyl ether. The product was purified by dissolving it in dichloromethane, filtering, and reprecipitating the solid by the addition of ethyl ether (yield, 70%).

$[Ir_2(SbF_2)(CO)_2Cl_2(\mu\text{-dpma})_2](BF_4)$. A solution of 63 mg of $Ir_2(CO)_2Cl_2(\mu\text{-dpma})_2$ dissolved in 20 mL of dichloromethane was stirred over solid antimony(III) fluoride. The canary yellow solution immediately turned bright pink. After being stirred for 20 min, the solution was filtered through Celite and placed over solid sodium tetrafluoroborate. After 10 min of stirring, the solution was again filtered through Celite and the volume reduced to 10 mL. Addition of pentane caused the product to precipitate; yield 72 mg, 89%. The corresponding hexafluorophosphate salt was prepared similarly by using ammonium hexafluorophosphate in place of sodium tetrafluoroborate.

Physical Measurements. The $^{31}P\{^1H\}$ NMR spectra were recorded on a General Electric QE-300 NMR spectrometer that operates at 121.7 MHz with an external 85% phosphoric acid standard and the high-field positive convention for reporting chemical shifts. Infrared spectra were recorded on an IBM IR32 spectrometer. Electronic spectra were recorded with a Hewlett-Packard 8450A spectrometer. Uncorrected emission spectra were obtained through the use of a Perkin-Elmer MPF-44B fluorescence spectrometer.

Standard laser-induced fluorescence (LIF) techniques were employed to measure excited-state lifetimes with a Lambda Physik EMG 50 dye laser pumped by a Lambda Physik EMG 50 eximer laser operating on the XeCl transition with a pulse duration of 10 ns at 17 μJ per pulse. Emitted light was collected with a 4-in. parabolic mirror and focused into an Acton VM-510 1-meter monochromator. Emissions were monitored at their λ_{max} of emission. Luminescence was detected by a Hamamatsu R928 PMT. Output was directed to a EG&G Model 162 Boxcar averager. Scans were collected over a 20-μm range and averaged for 100 s with an average gate width of 5 ns. Intensity traces were collected on a X-Y recorder where they were analyzed for first-order decay over at least 10 half-lives. In each case the solvent was CH_2Cl_2 freshly distilled from CaH_2. Sample concentration were on the order of 10^{-1} M. Solvent was degassed by using four freeze–pump–thaw cycles.

X-ray Data Collection. $[Ir_2(PbI)(CO)_2I_2(\mu\text{-dpma})_2](PF_6)\cdot CH_2Cl_2$. Red crystals were obtained by slow diffusion of diethyl ether into a dichloromethane solution of $[Ir_2(PbI)(CO)_2I_2(\mu\text{-dpma})_2](PF_6)$. They were coated with a light hydrocarbon oil to prevent cracking upon exposure to air. The crystal was mounted on a glass fiber with silicon grease and placed into the 130 K nitrogen stream of a Syntex $P2_1$ diffractometer with a modified LT-1 low-temperature apparatus. Unit cell parameters were determined by least-squares refinement of 12 reflections with $11.6 < 2\theta < 24.9$. The axial lengths and triclinic crystal system were verified by examination of axial photos. The two check reflections showed only random fluctuations (<2%) in intensity throughout the data collection. The data were corrected for Lorentz and polarization effects. Crystal data are given in Table V.

$[Ir_2(SbF_2)(CO)_2Cl(\mu\text{-dpma})_2](BF_4)$. Crystals were obtained with difficulty by diffusion of pentane into a dichloromethane solution of the complex over a 2-week period. The crystals were immersed in a hydrocarbon oil to prevent cracking and a suitable prismatic crystal was chosen from the array of needle and prismatic crystals available. Data collection procedures followed those outlined above and crystal data are given in Table V. Based on the observed conditions, $h0l$, $h + l = 2n$; $hk0$, $k = 2n$, two space groups, $Pmnb$ (No. 62) and $P2_1nb$ (No. 33), were possible.

Solution and Structure Refinement. $[Ir_2(PbI)(CO)_2I_2(\mu\text{-dpma})_2](PF_6)\cdot CH_2Cl_2$. Calculations were performed on a Microvax computer with SHELXTL PLUS 4.11 software. Scattering factors and corrections for anomalous dispersion were taken from a standard source.[25] Successful solution and refinement of the structure was obtained in the centrosymmetric space group $P\bar{1}$. The positions of the iridium atoms were determined via the Patterson method. All non-carbon atoms excluding O(1), O(2), Cl(1), and Cl(2) were refined with anisotropic thermal parameters while all others were refined with isotropic thermal parameters. Hydrogen atoms were fixed to all carbon atoms where chemically justified. The hydrogen atom positions were calculated by using a riding model with C–H vector fixed at 0.96 Å and a thermal parameter 1.2 times that of the adjacent carbon atom. The structure refined to $R = 5.89\%$ ($R_w = 5.72\%$) by using 456 least-squares parameters and 12670 reflections. The goodness of fit was calculated at 1.31 with a mean shift/esd of 0.001 for the overall scale. An absorption correction was applied.[26]

$[Ir_2(SbF_2)(CO)_2Cl_2(\mu\text{-dpma})_2](BF_4)$. The structure was solved by Patterson methods in the space group $Pmnb$. Refinement followed procedures outlined above. The BF_4^- anion was badly disordered and no reasonable model for the disorder was found, although several were tried. Finally, a few atoms were included in the region where the BF_4^- group obviously resides, but a complete anion is not described in the final structural model. An absorption correction was applied.[26] Final refinement was carried out with anisotropic, thermal parameters for atoms of Ir, Sb, As, Cl, and P and isotropic parameters for other atoms. There are six peaks ranging from 2.4 to 1.4 $eÅ^{-3}$ in the region of the BF_4^- group in the final difference map. All the remaining features in the map are smaller and have no chemical significance. The largest shift in the final cycle of refinement was 0.12 for y of C(39).

Acknowledgment. We thank the National Science Foundation (CHE-894209) for support, Dr. R. Rosenfeld for access to equipment, and Johnson Matthey, Inc. for a loan of iridium salts. The diffraction and computing equipment used in this study were purchased under NSF Grant CHE-8802721 to the University of California, Davis.

Supplementary Material Available: Tables of atomic coordinates, bond distances, bond angles, anisotropic thermal parameters, hydrogen atom positions and crystal refinement data for $[Ir_2(PbI)(CO)_2I_2(\mu\text{-dpma})_2](PF_6)\cdot CH_2Cl_2$ and $[Ir_2(SbF_2)(CO)_2Cl_2(\mu\text{-dpma})_2](BF_4)$ (19 pages); listing of observed and calculated structure factors (69 pages). Ordering information is given on any current masthead page.

(25) *International Tables of X-ray Crystallography*; Kynoch Press: Birmingham, England, 1974; Vol. 4.

(26) The method obtains an empirical absorption tensor from an expression relating F_o and F_c: Moezzi, B. Ph.D. Thesis, University of California, Davis, 1987.